THE JOURNAL OF PHYSICAL CHEMISTRY B

Article

Cite This: J. Phys. Chem. B 2019, 123, 8074−8085

pubs.acs.org/JPCB

Ab Initio Investigation of the Resonance Raman Spectrum of the Hydrated Electron

Saswata Dasgupta, Bhaskar Rana, and John M. Herbert*

Department of Chemistry and Biochemistry, The Ohio State University, Columbus, Ohio 43210, United States

Supporting Information

ABSTRACT: According to the conventional picture, the aqueous or "hydrated" electron, e^-(aq), occupies an excluded volume (cavity) in the structure of liquid water. However, simulations with certain one-electron models predict a more delocalized spin density for the unpaired electron, with no distinct cavity structure. It has been suggested that only the latter (non-cavity) structure can explain the hydrated electron's resonance Raman spectrum, although this suggestion is based on calculations using empirical frequency maps developed for neat liquid water, not for e^-(aq). All-electron *ab initio* calculations presented here demonstrate that both cavity and non-cavity models of e^-(aq) afford significant red-shifts in the O−H stretching region. This effect is nonspecific and arises due to electron penetration into frontier orbitals of the water molecules. Only the conventional cavity model, however, reproduces the splitting of the H−O−D bend (in isotopically mixed water) that is observed experimentally and arises due to the asymmetric environments of the hydroxyl moieties in the electron's first solvation shell. We conclude that the cavity model of e^-(aq) is more consistent with the measured resonance Raman spectrum than is the delocalized, non-cavity model, despite previous suggestions to the contrary. Furthermore, calculations with hybrid density functionals and with Hartree−Fock theory predict that non-cavity liquid geometries afford only unbound (continuum) states for an extra electron, whereas in reality this energy level should lie more than 3 eV below vacuum level. As such, the non-cavity model of e^-(aq) appears to be inconsistent with available vibrational spectroscopy, photoelectron spectroscopy, and quantum chemistry.

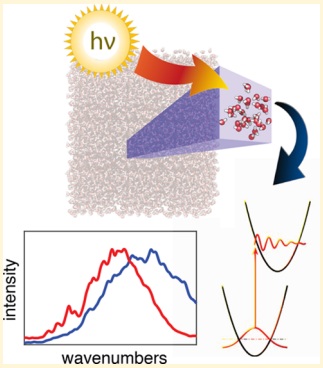

1. INTRODUCTION

Fundamental interest in the aqueous or "hydrated" electron,[1] e^-(aq), has been revived in recent years by questions regarding the veracity of the canonical "cavity model" of this species.[2−15] According to this model, the thermalized electron occupies an excluded volume in the structure of liquid water, as shown in Figure 1, where it forms hydrogen bonds to several water molecules, coordinating to a single O−H moiety of each.[1] This picture is supported by *ab initio* molecular dynamics (MD) simulations at a variety of levels of theory,[16−23] as well as by simulations based on one-electron pseudopotential models,[24−33] the latter of which facilitate much better sampling as compared to *ab initio* MD.

However, this simple picture has been repeatedly questioned by Schwartz and co-workers,[2,5,9−15] based on results from a pseudopotential model developed by Larsen, Glover, and Schwartz (LGS).[2] Simulations of e^-(aq) using the LGS model afford a very different picture in which no excluded volume is formed at all, and instead the spin density delocalizes over several water molecules with a slight enhancement of the water density near the centroid of the one-electron wave function. The essential structural differences between this picture and the canonical cavity model are captured by Figure 2, which depicts the one-electron wave function obtained from a simulation with the LGS pseudopotential model, in comparison to the spin density obtained from a cavity-forming pseudopotential model.

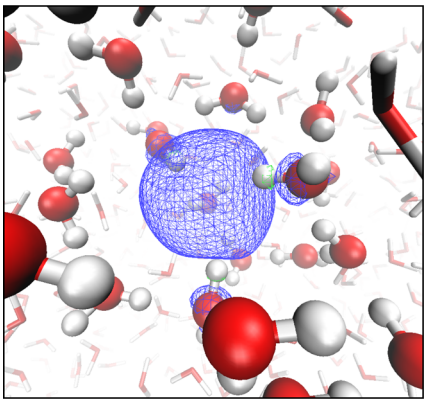

Figure 1. Spin density ($\rho_{spin} = \rho_\alpha - \rho_\beta$) of e^-(aq), illustrating the canonical "cavity model" of this species. The isocontour that is plotted contains 92% of ρ_{spin}, and the extremely small regions of green mesh indicate where $\rho_{spin} < 0$. These regions are confined to the O−H moieties that are coordinated directly to e^-(aq). Reprinted from ref 23. Copyright 2019 American Institute of Physics.

Although various aspects of the LGS model have been criticized,[3,4,6−8] there are a few experimental features of e^-(aq) that are described (at least qualitatively) by this model, but

Received: May 23, 2019
Revised: August 21, 2019
Published: August 23, 2019

DOI: 10.1021/acs.jpcb.9b04895
J. Phys. Chem. B 2019, 123, 8074−8085

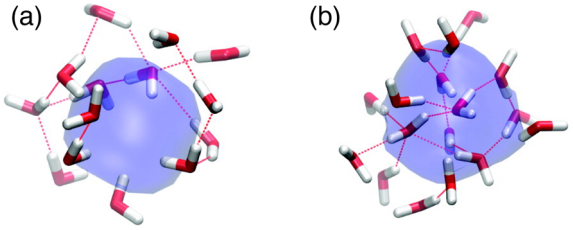

Figure 2. Ground-state e^-(aq) wave functions and nearby water molecules from simulations using (a) the cavity-forming pseudopotential model developed by Jacobson and Herbert[31] and (b) the non-cavity-forming LGS model.[2] Both simulations were performed in bulk water but only water molecules within 4.5 Å of the electron's center of mass are shown. Isosurfaces encapsulate 70% of $|\psi(\mathbf{r})|^2$. Reprinted from ref 6. Copyright 2011 American Chemical Society.

which have not been satisfactorily explained or reproduced within the cavity model of this species.[9−13] An important one is the resonance Raman (RR) spectrum,[34−38] which Schwartz and co-workers call "the best experimental indicator of the hydrated electron's structure".[12] Relative to the normal (ground-state) Raman spectrum of neat liquid water, the RR spectrum of e^-(aq) is down-shifted and considerably broadened on the low-energy side,[36] as shown in Figure 3.

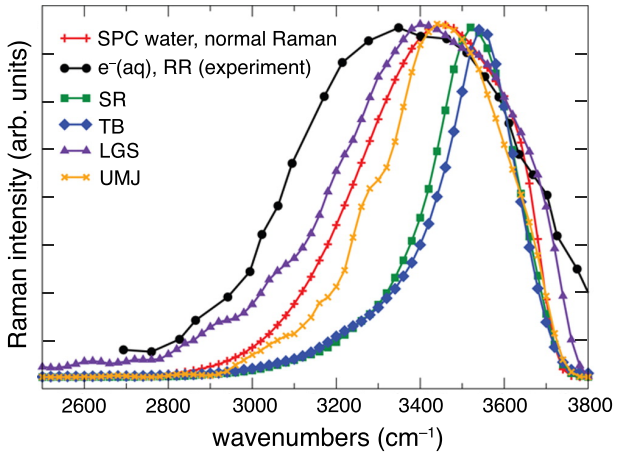

Figure 3. Experimental RR spectrum of e^-(aq) (in black, from ref 36), along with predictions from various theoretical models. These include the Schnitker−Rossky[24,39] (SR) and Turi−Borgis[26,40] (TB) pseudopotential models, which are cavity-forming, along with the non-cavity-forming Larsen−Glover−Schwarz[2] (LGS) model. The underlying water model in each case is the "flexible SPC" model,[41] and its Raman spectrum (representing neat liquid water) is shown in red. This is computed using the same frequency map (eq 1) that is used to compute the RR spectra of e^-(aq). The Uhlig−Marsalek−Jungwirth (UMJ) result uses structural snapshots from a cavity-forming DFT simulation,[18] in conjunction with the frequency-map approach. Adapted from ref 10. Copyright 2013 American Chemical Society.

Simulations using the LGS model afford a RR spectrum for e^-(aq) that is a bit broader than the normal Raman spectrum of neat liquid water,[9] if the latter is computed using the water force field that underlies the model. The peak of the LGS spectrum is *slightly* red-shifted with respect to the neat water spectrum, by perhaps 50 cm^{-1}. Experimentally, the red-shift with respect to the neat solvent is ≈200 cm^{-1},[36] a fact that is not evident from the data presented in Figure 3.

Simulations performed using the cavity-forming Turi−Borgis[26,40] (TB) and Schnitker−Rossky[24,39] (SR) pseudopotential models afford RR spectra that are even narrower than that of the neat solvent, as shown in Figure 3. (The TB, SR, and LGS models are each built upon the same "flexible SPC" water model,[41] so their RR spectra should be compared to the normal Raman spectrum for SPC water, which is depicted in red in Figure 3.) Furthermore, the TB and SR spectra of e^-(aq) are shifted to somewhat *higher* frequencies as compared to the Raman spectrum of the underlying water model,[9] in conflict with experiment. These observations have been used by Schwartz and co-workers to criticize the prevailing, cavity-centric viewpoint.[9,10]

It is worth noting, however, that the RR spectra in Figure 3 were not computed using all-electron quantum chemistry.[9] This is especially significant given that the usual mechanism for vibrational red-shifts in anion···water complexes is charge penetration from the anion into σ* orbitals on the O−H moieties that are hydrogen-bonded to it,[42−44] an effect that is absent in one-electron models of e^-(aq). Quantum chemistry calculations of the RR spectrum of e^-(aq) are reported here for the first time, although RR spectra of small $H_3O(H_2O)_n$ clusters have been reported previously.[45,46] Such clusters exhibit a high degree of $H_3O^+\cdots e^-$ charge separation and thus manifest many of the spectroscopic features associated with the hydrated electron.[45−49]

In contrast, the RR spectra computed by Schwartz and co-workers[9,10] (Figure 3) were computed using a "transition frequency map" developed by Corcelli et al. for neat liquid water.[50,51] Those authors discovered an empirical relationship between the local electric field along an O−H bond vector (in a classical MD simulation of liquid water) and the anharmonic O−H vibrational frequency computed (using quantum chemistry) for small water clusters extracted from classical simulations. Similar maps were developed for the polarizability of a water molecule,[51,52] and a formula

$$\omega(F_{OH}) = c_0 + c_1 F_{OH} + c_2 F_{OH}^2 \quad (1)$$

was parametrized for the O−H fundamental frequency (ω) as a function of the field strength (F_{OH}) measured in a classical simulation.[52] This "frequency map" provides a means to obtain the instantaneous O−H oscillator frequencies for any water molecule in a simulation, which is useful since the time correlation function of the frequency fluctuations can be related to vibrational line shape.[50−52]

Although this approach has been applied successfully to predict infrared and Raman line shapes in neat liquid water and in ice,[50−53] its application to e^-(aq) is untested beyond the fact that it results in a somewhat broadened RR spectrum for the LGS model of e^-(aq). To apply eq 1 in that context, the electric field arising from the one-electron wave function must be added to that arising from the classical water molecules, and then to obtain the RR spectrum the frequency obtained from eq 1 is weighted by the difference in ground- and excited-state gradients. This difference constitutes the RR enhancement factor,[54] as discussed in section 2.1. The parameters in eq 1, which were developed to describe neat liquid water, were not modified for use with e^-(aq).[9] Despite these concerns about how the RR spectra were modeled, it is certainly provocative that such distinct differences are observed between the cavity and non-cavity models.

In the present work, we investigate the RR spectra afforded by various structural models of e^-(aq) using all-electron

DOI: 10.1021/acs.jpcb.9b04895
J. Phys. Chem. B 2019, 123, 8074−8085

quantum chemistry, within the excited-state gradient approximation.[55−57] (This is equivalent to the short-time approximation pioneered by Heller and co-workers.[58,59]) In this approach, the RR spectrum is obtained from the excited-state gradient projected onto ground-state normal modes, which can be computed using density functional theory (DFT) for sizable models of e^-(aq). The difference between this procedure and the force-weighting approach used by Schwartz and co-workers[9,10,12] is that, in the present work, vibrational frequencies and normal Raman intensities are obtained from electronic structure calculations on *all-electron* models of e^-(aq), which therefore contain the proper physics to describe the molecular-level origins of O−H vibrational red-shifts.[44] This sidesteps the uncertainty associated with using a frequency map designed for neat liquid water in the conjunction with electric fields from e^-(aq) that are probably unlike anything in the data set that was used to parametrize eq 1. In addition, there exists no frequency map for the bending region of the vibrational spectrum, whereas experimental RR spectra for e^-(aq) in the bending region afford important structural information.[36] Theoretical calculations of the RR spectrum of e^-(aq) in the bending region are presented here for the first time.

2. METHODS

2.1. Theory. The theory of RR scattering and its historical development are summarized by Myers,[60,61] and modern implementations are discussed in more recent papers.[55−57,62−65] In principle, the theory is fully described by the Kramers−Heisenberg−Dirac dispersion formalism based on the Raman polarizability tensor,[61]

$$\alpha_{\sigma\tau}(\omega_L, \omega_S) = \sum_v \left[\frac{\langle f|\hat{r}_\sigma|v\rangle\langle v|\hat{r}_\tau|i\rangle}{\hbar\omega_L - \hbar\omega_{vi} + \imath\Gamma_{iv}} + \frac{\langle f|\hat{r}_\tau|v\rangle\langle v|\hat{r}_\sigma|i\rangle}{\hbar\omega_{vi} + \hbar\omega_S + \imath\Gamma_{iv}} \right] \tag{2}$$

Here, $|i\rangle$ and $|f\rangle$ represent initial and final states, respectively; ω_L is the frequency of the incident photon (laser); and ω_S is the frequency of the scattered photon. Equation 2 is inconvenient due to the sum over intermediate states v representing vibrational levels on all accessible electronic states. The usual procedure is to expand the static molecular polarizability as a Taylor series in the normal vibrational coordinates,[66−68] which allows the Raman intensity to be decomposed into Franck−Condon contributions ("A term") and coordinate-dependent Herzberg−Teller contributions (B and C terms).[61,66,67,69] Nevertheless, each term contains sums over intermediate vibrational states and becomes difficult to evaluate for large molecules with numerous vibrational modes.

The time-dependent picture provides an alternative means to derive RR intensities.[58,59] In this approach, the requisite polarizability tensor elements involving different electronic states (eq 2) are expressed in terms of the Fourier transform of the overlap between the time-evolving wave packet $|\Psi(t)\rangle$ and the final-state wave function $|\psi_f\rangle$:

$$\alpha(\omega_L) \propto \int_0^\infty e^{\imath\omega_L t - \Gamma t}\langle\psi_f|\Psi(t)\rangle dt + \text{NRT} \tag{3}$$

Here, NRT indicates the nonresonant terms that are neglected in RR spectroscopy. Large molecules likely spend no more than 10−20 fs in the Franck−Condon region, and the overlap $\langle\psi_f|\Psi(t)\rangle$ is probably only significant on that time scale.[54,59] As such, a short-time approximation can be applied wherein the relevant quantity is the slope of the excited-state potential surface, evaluated at the ground-state geometry. In principle one should consider the effects of Duschinsky rotation,[70,71] i.e., the fact that the normal coordinates are different in each electronic state. Neglecting this effect for simplicity and thus using ground-state normal modes only, one arrives at the independent-mode, displaced harmonic oscillator (IMDHO) model of RR spectroscopy.[55−57,62−65]

Within an IMDHO model and considering only two electronic states, the RR intensity I_k for normal mode k is[72,73]

$$I_k \propto \omega_L(\omega_L - \omega_k)^3(\omega_k\Delta_k)^2 \tag{4}$$

Here, ω_k is the ground-state vibrational frequency, which is the same as the excited-state frequency within the IMDHO approximation. The quantity

$$\Delta_k = \left(\frac{\omega_k}{\hbar}\right)^{1/2}\Delta Q_k \tag{5}$$

is the dimensionless displacement of the kth mode in the excited state,[57] expressed in terms of the displacement ΔQ_k in the mass-weighted normal mode displacement coordinate, Q_k. Within the IMDHO approximation, the displacement Δ_k can be computed from the gradient $\partial\Omega/\partial Q_k$ of the electronic excitation energy, Ω:[57]

$$\Delta_k = -\frac{1}{\sqrt{\hbar\omega_k^3}}\left(\frac{\partial\Omega}{\partial Q_k}\right)\Bigg|_{\mathbf{Q}=\mathbf{0}} \tag{6}$$

The derivative is evaluated at the ground-state geometry ($\mathbf{Q} = \mathbf{0}$). Since $\omega_L \gg \omega_k$ in eq 4, the RR intensity ratio for two different normal modes can be expressed as[57,65,72]

$$\frac{I_j}{I_k} = \left(\frac{\omega_j\Delta_j}{\omega_k\Delta_k}\right)^2 \tag{7}$$

In view of eqs 6 and 7, the IMDHO approach to RR spectroscopy is known synonymously as the excited-state gradient approximation.[55,73]

Next introduce the Hessian matrix $\mathbf{K}$ in mass-weighted Cartesian coordinates, $q_\alpha = m_\alpha^{1/2}x_\alpha$. The solution to the ground-state normal mode problem,

$$\mathbf{L}^\dagger\mathbf{K}\mathbf{L} = \boldsymbol{\lambda} \tag{8}$$

affords a diagonal matrix of eigenvalues $\lambda_k = \omega_k^2$. The matrix $\mathbf{L}$ represents the transformation from mass-weighted Cartesian coordinates q_α to mass-weighted normal mode coordinates Q_k. Assuming identical frequencies in the ground and excited states, one obtains a linear transformation between the displacements expressed in normal coordinates and the those in Cartesian coordinates:[63]

$$\boldsymbol{\Delta}_\mathbf{Q} = \lambda^{-1}\mathbf{L}^\dagger\mathbf{M}^{-1/2}\mathbf{V}_\mathbf{x} \tag{9}$$

The matrix $\mathbf{M}$ is diagonal and contains the atomic masses m_α, and $\mathbf{V}_\mathbf{x}$ is the excited-state difference gradient expressed in Cartesian coordinates. The latter consists of the Cartesian derivatives of the excitation energy, $\partial\Omega/\partial x_\alpha$. Using eq 5 in conjunction with $\lambda_k = \omega_k^2$, the ratio of displacements that is needed in eq 7 is

DOI: 10.1021/acs.jpcb.9b04895
J. Phys. Chem. B 2019, 123, 8074−8085

$$\frac{\Delta_j}{\Delta_k} = \left(\frac{\lambda_j}{\lambda_k}\right)^{1/4} \frac{(\mathbf{\Delta_Q})_j}{(\mathbf{\Delta_Q})_k} \tag{10}$$

2.2. Computational Details. All RR calculations reported in this work are performed within the IMDHO approximation using the excited-state gradient method described above, which we have implemented in a locally modified version of the Q-Chem program.[74] Ground-state harmonic frequencies are computed using either DFT or Hartree−Fock (HF) theory, and then excitation energies are computed using either time-dependent (TD-)DFT or, in the case of normal-mode analysis at the HF level, configuration interaction singles (CIS).

Given the solvent-supported nature of e^-(aq), it is not obvious that spectra computed at relaxed, ground-state local minima would provide a complete picture. Instead, we perform normal-mode analysis (eq 8) on snapshots taken from MD trajectories, without relaxing the geometries of those snapshots. This procedure is the hallmark of the "instantaneous normal modes" (INM) theory of liquids.[75,76] The spectrum of eigenvalues λ_k obtained at unrelaxed geometries includes "unstable modes" (in INM parlance) characterized by imaginary frequencies, and for liquid water the spectrum of unstable modes typically extends to 400−800$\imath$ cm^{-1} along the imaginary axis.[76−79] Nevertheless, in classical simulations of liquid water, the INM spectrum agrees reasonably well with the power spectrum obtained from the velocity autocorrelation function.[78,79] Importantly, there is a clear separation of energy scales between the bending modes and the translations and hindered rotations, the latter of which are mixed in with the unstable modes.[77−79] The unstable modes contain information about fluctuations in the hydrogen-bonding network,[80] but in the present work we are interested only in stretching and bending frequencies.

INM spectra of liquid water have also been reported using a DFT-based QM/MM protocol.[81] As with the classical simulations, these spectra are in reasonable agreement with the density of states obtained from the velocity autocorrelation function and furthermore exhibit a clear separation of energy scales between the bending modes and the terahertz part of the spectrum (ω < 1000 cm^{-1}).[81] INM analysis has also been reported for e^-(aq),[80] based upon a cavity-forming one-electron pseudopotential model. Similar to the case of neat liquid water, the density of unstable modes extends out to $\omega \sim 500\imath$ cm^{-1} and the bending part of the spectrum terminates above 1500 cm^{-1}, well outside of the terahertz region. Given the energy gap, we do not anticipate mode-mixing between the bending modes of interest and the unstable modes at lower energies.

Using the excited-state gradient formalism, RR intensities are computed at each snapshot along a trajectory, and then the snapshots are combined to obtain an ensemble-averaged RR spectrum. In so doing, we apply a Lorentzian broadening of 45 cm^{-1} to the "stick spectra" obtained from the individual snapshots. For an example of a stick spectrum without this broadening, see Figure S1 in the Supporting Information.

This procedure was carried out for snapshots of the liquid structure obtained from several different simulations. First, we consider a trajectory generated using the LGS pseudopotential model, obtained from simulations reported in refs 4 and 6. Second, we consider a trajectory obtained from DFT-based QM/MM simulations reported by Uhlig, Marsalek, and Jungwirth (UMJ).[18] The latter simulations employed 32 QM water molecules and 992 MM water molecules in a periodic cell, using the BLYP+D3 functional with an empirical self-interaction correction that was originally parametrized for the aqueous hydroxyl radical.[82] Snapshots from this UMJ trajectory were also used by Schwartz and co-workers in their frequency-map approach;[10] see Figure 3.

Finally, we have pursued a more consistent approach in which frequency calculations are performed at the same level of theory that is used to propagate the trajectory. Following our own recent work,[23] we propagated a QM/MM trajectory at the level of HF+D3/3-21++G*, i.e., Hartree−Fock theory plus Grimme's empirical "+D3" dispersion correction.[83] These calculations include 24 water molecules in the QM region and another 1000 MM water molecules in a periodically replicated simulation cell. Simulations reported previously demonstrate that this level of theory is sufficient to stabilize an excluded-volume structure for e^-(aq).[23] In particular, electron correlation is not required in order to maintain a stable cavity structure. The cavity remains stable in periodic liquid simulations performed at the level of second-order Møller−Plesset perturbation theory (MP2).[22]

Examination of the RDFs for various models of e^-(aq) suggests that two full solvation shells are contained within a radius of ≈5.5 Å around the centroid of the spin density.[6,18,23] In snapshots extracted from the simulations described above, we therefore include at the QM level all H_2O molecules within a radius R_{QM} = 5.5 Å of the centroid of the spin density. For the cavity-forming models, this amounts to ≈24 water molecules, although the precise number varies from one snapshot to the next. When the snapshots are extracted from the LGS simulation, the same radius encompasses ≈35 water molecules. In either case, this QM region is then surrounded by a much larger number of classical point charges. This procedure is depicted schematically in Figure 4.

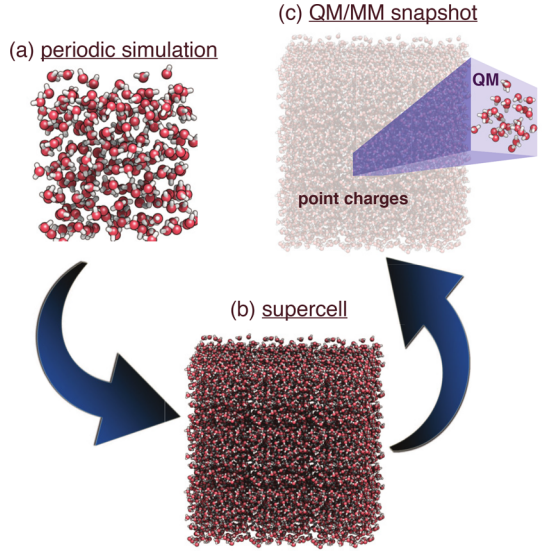

Figure 4. Schematic view of how water molecules are selected for inclusion in QM/MM snapshots used to generate RR spectra. (a) Following a simulation carried out with periodic boundary conditions, (b) a supercell is created and (c) a QM region is delineated that includes all water molecules within a specified radius (R_{QM}) of the centroid of the e^-(aq) spin density. The remaining water molecules in the supercell are described using classical point charges.

DOI: 10.1021/acs.jpcb.9b04895
J. Phys. Chem. B 2019, 123, 8074−8085

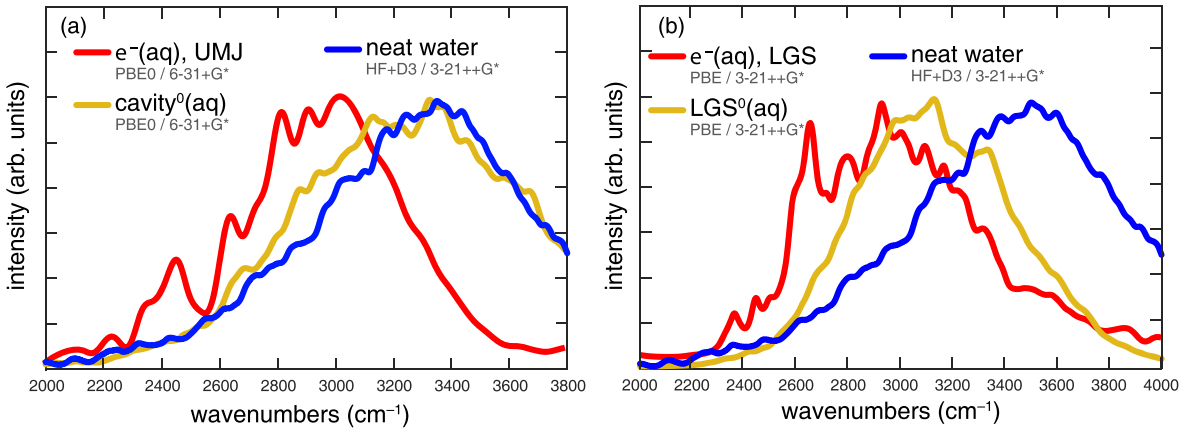

Figure 5. Ensemble-averaged resonance Raman intensities for e^-(aq) and normal Raman spectra of neat water. These geometries are taken from (a) the cavity-forming, DFT-based QM/MM simulations reported by UMJ[18] and (b) non-cavity simulations using the LGS pseudopotential. RR calculations in (a) are performed at the (TD-)PBE0/6-31+G* level of theory, while those in (b) are performed at the (TD-)PBE/3-21++G* level of theory, for reasons discussed in the text. Spectra labeled "cavity^0(aq)" and "LGS^0(aq)" are the Raman spectra of the *neutral* liquid obtained from the UMJ and LGS trajectories upon removing the extra electron; the cavity^0(aq) data in (a) thus correspond to the normal Raman spectrum of an empty cavity in liquid water. Also shown in both panels is the normal Raman spectrum for neat liquid water computed at the HF+D3/3-21++G* level using snapshots from a QM/MM simulation at the same level of theory.

Normal modes for these QM/MM snapshots of e^-(aq) are computed at various levels of quantum chemistry including PBE0/6-31+G*, PBE/3-21++G*, and HF+D3/3-21++G*. The excited-state gradient is computed (at the TD-DFT or CIS level) using the same functional and basis set, and this information is used to compute the RR enhancement factors as described in section 2.1. A normal Raman spectrum for liquid water is computed using the same procedure to extract QM/MM snapshots from a trajectory, and Raman intensities are computed as part of the usual ground-state normal-mode analysis. The same line-broadening and ensemble-averaging procedure is applied to the stick spectra for both the RR and the normal Raman spectra.

Regarding basis sets, we have previously established that in liquid water a single set of atom-centered diffuse functions is sufficient to represent e^-(aq) in a cavity.[6,23,30] In contrast, such basis sets are *not* adequate for gas-phase $(H_2O)_n^-$ clusters, where additional diffuse functions are needed to avoid artifacts.[84,85] Note also that the standard 3-21G* basis set from which 3-21++G* is constructed does not include polarization functions for second-row atoms (e.g., oxygen), nevertheless a stable cavity is maintained at the HF+D3/3-21++G* level.

3. RESULTS

3.1. Raman Spectra in the O−H Stretch Region. Figure 5a presents the RR spectrum computed at the PBE0/6-31+G* level using liquid geometries obtained from the cavity-forming, DFT-based UMJ trajectory. This spectrum is computed from a total of 86 individual snapshots, each separated in time by 100 fs. Fluctuations or "wiggles" in the spectral envelope result from heterogeneity in the ensemble average and can be made to disappear if the stick spectra (obtained from DFT harmonic frequency calculations) are broadened by more than the 45 cm^{-1} that is used here.

Plotted alongside the RR spectrum for e^-(aq) in Figure 5a are ground-state Raman spectra for two different neutral water systems. One of these is simply neat liquid water, where snapshots were obtained from a QM/MM simulation at the HF+D3/3-21++G* level. This is a different level of theory, with different harmonic frequencies, as compared to the PBE0/6-31+G* calculations used to obtain the RR spectrum of e^-(aq) in Figure 5a. As a result, although the e^-(aq) spectrum is red-shifted relative to the neat liquid spectrum, it is not clear *a priori* how much of this shift arises simply from this change in the level of theory. To address this, we performed harmonic frequency calculations at the PBE0/6-31+G* level on the same UMJ snapshots used to compute the RR spectrum for e^-(aq), but treating these snapshots as charge-neutral systems, omitting the extra electron. The ensemble-averaged, ground-state Raman spectrum obtained from these snapshots is labeled "cavity^0(aq)" in Figure 5a. It is the Raman spectrum of the empty, charge-neutral cavity in liquid water that is obtained from the UMJ snapshots, and it is not significantly different from the spectrum of neat liquid water that we compute at the HF+D3/3-21++G* level.

As a further comparison, we examined harmonic frequencies for a water hexamer at both of the aforementioned levels of theory. HF+D3/3-21++G* frequencies for the O−H stretching modes in $(H_2O)_6$ range from 3001−3983 cm^{-1}, versus a range of 3085−3930 cm^{-1} at the PBE0/6-31+G* level. These differences are relatively small in comparison to the breadth of the O−H stretching band in the liquid, which justifies comparison between unscaled harmonic frequencies from these two different levels of theory. We conclude that all or most of the red-shift between the RR spectrum for e^-(aq), and the normal Raman spectrum for liquid water, arises from the presence of the electron and not from changes in the liquid structure or details of the theoretical treatment.

We next wish to present a similar comparison using snapshots extracted from non-cavity LGS simulations in place of UMJ snapshots. In attempting to duplicate the same level of theory, however, we discovered that the singly-occupied molecular orbital (SOMO) energy level is unbound ($\varepsilon_{SOMO} > 0$) at the PBE0+D3/6-31+G* level of theory, when the liquid geometries used to model e^-(aq) are extracted from simulations using the LGS pseudopotential. This is true for nearly all QM/MM snapshots that are extracted with a radius R_{QM} = 5.5 Å, as in the calculations described above. For LGS liquid geometries, this radius encompasses ≈35 QM water

DOI: 10.1021/acs.jpcb.9b04895
J. Phys. Chem. B 2019, 123, 8074−8085

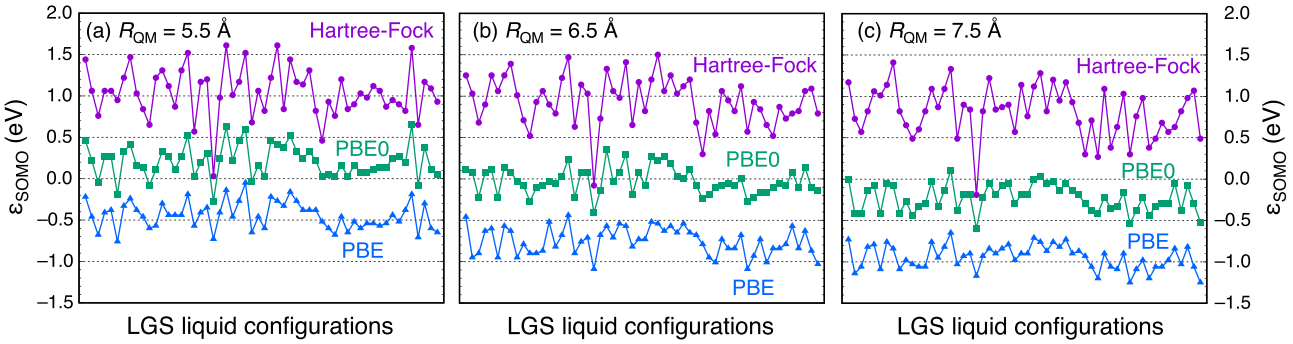

Figure 6. Plots of the SOMO eigenvalue (ε_{SOMO}) for e^-(aq), based on single-point QM/MM calculations at liquid geometries extracted from a simulation using the LGS pseudopotential. Calculations were performed at either the HF+D3/6-31+G*, PBE0+D3/6-31+G*, or PBE+D3/3-21++G* level of theory (as indicated), using three different radii (R_{QM}) for the QM region.

molecules, and Figure 6a presents the distribution of ε_{SOMO} levels obtained from these QM/MM snapshots using the HF and PBE functionals in addition to PBE0. At the HF+D3/6-31+G* level, every single snapshot corresponds to an unbound state, typically with ε_{SOMO} = +0.5−1.5 eV.

The SOMO level can be stabilized somewhat by increasing the size of the QM region, which increases the magnitude of the electron−water polarization interaction. Using R_{QM} = 6.5 Å (Figure 6b), the PBE0 SOMO is stabilized to the point that it teeters on the brink of becoming a bound state. It finally does become bound when R_{QM} = 7.5 Å (Figure 6c), in *almost* all of the snapshots. The electron−water polarization interaction appears to have largely saturated by R_{QM} = 7.5 Å, for which the snapshots contain an average of 75 QM water molecules. It is possible that larger QM regions *might* convert all of the PBE0 snapshots into bound states but it is unlikely that the same would be true for HF calculations carried out on the same snapshots. Even with R_{QM} = 7.5 Å, the HF energy level remains unbound by a significant amount, with $\varepsilon_{SOMO} \gtrsim 0.5$ eV for nearly every snapshot.

According to HF theory, this result implies that the SOMO is actually a continuum state at typical LGS liquid geometries, and its wave function is therefore *completely* delocalized across the entire QM region, not simply the $r_{gyr} \approx 2.6$ Å region over which the one-electron LGS wave function extends. (An isosurface plot of one of these delocalized states can be found in Figure S3b.) Although the PBE0 functional binds the electron for most (though not all) of the R_{QM} = 7.5 Å LGS snapshots, this fact likely relies upon significant intervention from self-interaction error (i.e., delocalization error[86]). In contrast, the HF values of ε_{SOMO} contain the genuine stabilization effect of electron−water polarization but are free of artificial stabilization due to self-interaction.

That the LGS model predicts a strongly-bound electron at liquid geometries for which HF theory predicts an unbound state is a manifestation of the fact that the LGS pseudopotential is known to be overly attractive.[3,4,7,8] This fact makes us skeptical of the LGS model but it also complicates the analysis at hand, because these unbound states clearly should not be used to compute the RR spectrum. Note from Figure 6 that the semilocal PBE functional exhibits a bound-state SOMO in all snapshots, even for smallest QM region employed here. As a pragmatic workaround to obtain a sensible RR spectrum at LGS geometries, we therefore settle on the PBE functional. Operationally, the larger self-interaction error in this semilocal functional (as compared to the hybrid functional PBE0) artificially stabilizes ε_{SOMO} and thereby allows us to obtain a bound state whose RR spectrum can sensibly be computed using the methods employed here.

The RR spectrum of e^-(aq) computed at the (TD-)PBE/3-21++G* level of theory, using LGS snapshots, is shown in Figure 5b. Also shown is a Raman spectrum for neat liquid water as well as the "LGS^0(aq)" Raman spectrum, which uses liquid geometries from the LGS simulations, sans electron. The latter is analogous to what we called the cavity^0(aq) spectrum in the case of the UMJ geometries, except there is no cavity in the LGS case but rather an enhanced liquid density in the region formerly occupied by the unpaired electron. Perhaps for that reason, due to water molecules pushed closer together than they are in normal liquid water, the LGS^0(aq) Raman spectrum is noticeably red-shifted with respect to the neat water spectrum. In contrast to the situation with the UMJ geometries, in the LGS case some portion of the RR red-shift appears to arise from changes in the liquid structure upon electron solvation, in addition to the $e^- \rightarrow \sigma^*_{OH}$ charge-penetration effects that are present in both cases, when all-electron DFT calculations are used. The charge-penetration effect is fully responsible for the red-shift in the case of UMJ geometries, and this may explain why the RR spectrum at LGS geometries exhibits features further to the red of those observed in spectra computed at UMJ geometries, e.g., the peak around 2650 cm^{-1} in Figure 5b.

Here and elsewhere,[44] vibrational red-shifts in hydrated electrons are ascribed to $e^- \rightarrow \sigma^*_{OH}$ charge penetration, and one might wonder whether a more classical anion such as Cl$^-$(aq) exhibits the same behavior. However, the normal Raman spectrum of Cl$^-$(aq) is known to exhibit a very slight *blue*-shift as compared to that of neat liquid water,[87] and it is interesting to test whether the present computational methodology can capture this effect. Comparison between e^-(aq) and Cl$^-$(aq) is furthermore interesting insofar as the latter exhibits bond-oriented coordination in a solvent cavity that is comparable in size to that predicted by the cavity-forming models of e^-(aq).

In Figure 7, we compare the RR spectrum for e^-(aq) to the normal Raman spectra for Cl$^-$(aq) and for neat liquid water, each computed at a consistent level of theory (HF+D3/3-21++G*) using snapshots taken from QM/MM simulations at the same level of theory. Consistent with experiment, the Raman spectrum of Cl$^-$(aq) is slightly blue-shifted with respect to that of neat liquid water whereas the RR spectrum of e^-(aq) is significantly red-shifted. As compared to the spectra discussed above, the quantitative value of this shift is more meaningful

DOI: 10.1021/acs.jpcb.9b04895
J. Phys. Chem. B 2019, 123, 8074−8085

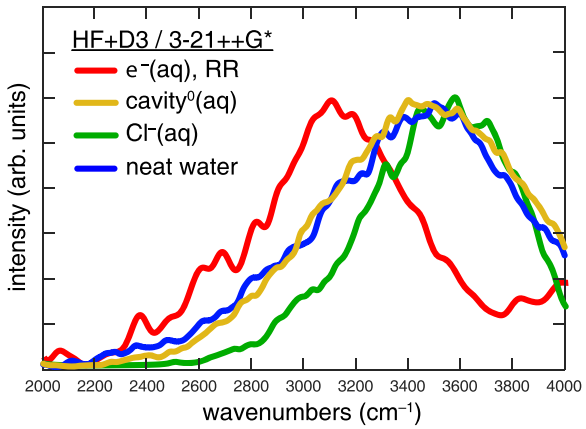

Figure 7. Resonance Raman spectrum for e^-(aq), and normal Raman spectra for the other species, computed at a consistent level of theory (namely, HF+D3/3-21++G*), using snapshots from QM/MM simulations at the same level of theory. The "cavity^0(aq)" spectrum is the Raman spectrum of the empty cavity left behind in liquid water when the unpaired electron is removed from the e^-(aq) snapshots.

here, given that all spectra are computed at the same level of theory. The down-shift that is reported experimentally is ≈200 cm^{-1} at half-maximum on the low-energy side of the O−H stretching feature,[36] and the spectra in Figure 7 are about right in that respect, albeit with a red-shift in the band maximum that is closer to 300 cm^{-1}.

The Raman spectrum of cavity^0(aq) in Figure 7 is also quite informative, as it is essentially indistinguishable from the Raman spectrum of neat liquid water. Very slight differences between these two spectra that were evident when UMJ geometries were used for cavity^0(aq) (Figure 5a) have vanished in this more consistent treatment. This provides compelling evidence that the red-shift in the RR spectrum of e^-(aq) originates in the same charge-penetration mechanism that is responsible for vibrational red-shifts in $(H_2O)_n^-$ clusters.[44] Absent the electron, slight differences in O−H stretching frequencies engendered by the presence of an empty cavity are washed out by the bulk liquid and cannot be seen in the Raman spectrum. Whereas frequency-map calculations (Figure 3) give the impression that the RR spectrum obtained from cavity-forming geometries is much too narrow in comparison to experiment,[9,10] when the e^-(aq) RR spectrum and the neat water Raman spectrum are computed at the same *ab initio* level of theory, a red-shift in the former emerges naturally.

3.2. Discussion and Critique. The frequency-map technique developed by Skinner and co-workers works very well for computing the vibrational line shapes in neat liquid water,[50−53] for which it was parametrized. However, the electric field that is experienced by O−H oscillators in the vicinity of a hydrated electron is likely significantly different from any data that were included in the training set for this model, so the use of this technique to compute RR spectra for e^-(aq) seems questionable. Moreover, since the UMJ snapshots came from a DFT calculation it seems much more consistent to compute the RR spectrum of these geometries using DFT frequency calculations.

We have performed such calculations here, and indeed we obtain a red-shift for the RR spectrum of e^-(aq) using UMJ geometries (Figure 5a). This shift is on the order of ∼300 cm^{-1}, somewhat larger than the experimental result (∼200 cm^{-1}),[36] but in comparison the frequency-map approach affords no shift whatsoever for the UMJ geometries and only ≈50 cm^{-1} when using LGS geometries. The larger value that we obtain is in line with vibrational red-shifts of ∼300 cm^{-1} that are measured experimentally in small $(H_2O)_n^-$ clusters.[88−92] These can be computed quantitatively using DFT,[89−91] and rationalized in terms of $e^- \rightarrow \sigma^*_{OH}$ charge penetration.[44] See ref 1 for a brief overview of the vibrational spectroscopy of $(H_2O)_n^-$ clusters.

Whereas our spectral calculations at UMJ geometries use a somewhat different level of theory as compared to the original QM/MM simulations by UMJ,[18] the red-shift remains when all calculations are performed at a consistent level of theory; see Figure 7. The latter calculations further support the notion of $e^- \rightarrow \sigma^*_{OH}$ charge penetration as the origin of the downshifted vibrational frequencies, since a charge-neutral cavity in liquid water exhibits no such shift as compared to the Raman spectrum of neat liquid water.

Although the ensemble-averaging procedure that is used here does not afford completely smooth spectral envelopes, Figure S4 of the Supporting Information demonstrates that all features of the experimental RR spectrum of e^-(aq),[36] from 500−4000 cm^{-1}, are reproduced semiquantitatively by our theoretical approach, at the level of theory that is used to generate the spectra shown in Figure 7. The comparison to experiment (Figure S4) does reveal that the frequencies are shifted due to limitations in the theory (primarily the fact that we make no attempt to include anharmonicity, and more generally the short-time IMDHO approach for computing the RR spectrum); nevertheless, the full spectrum is in remarkably good agreement with experiment. Figure S1 shows that the red-shift computed in the e^-(aq) spectrum is evident even in the "stick spectra" that come directly from the harmonic frequency calculations, and is therefore not an artifact of the broadening that we apply in order to obtain a continuous spectral envelope from an ensemble of snapshots.

Note that the diffusion constant of e^-(aq) is rather large, approximately the same as that of OH^-(aq),[93] and in QM/MM simulations this solute eventually drifts to the edge of the QM region as depicted in Figure S5. For QM regions of the size employed here, with a radius R_{QM} = 5.5 Å and including ≈24 water molecules, the spin density associated with e^-(aq) often drifts to the QM/MM boundary within the first 1−2 ps of dynamics,[23] at which point the trajectory becomes unusable. To circumvent this problem, while still obtaining sufficient data to generate a reasonably smooth spectral profile, the spectra shown in Figure 7 are generated from six different QM/MM trajectories that are each 1 ps in length. Spectra from each individual trajectory can be found in Figure S6, and in each case the RR spectrum of e^-(aq) is clearly red-shifted with respect to the Raman spectrum of neat liquid water.

Finally, let us return to fact that HF-based QM/MM calculations performed at LGS liquid configurations predict mostly unbound states ($\varepsilon_{SOMO} \gtrsim 0.5$ eV), even with as many as 75 QM water molecules included in the calculation (Figure 6). This stands in contrast to cavity models of e^-(aq), for which the energy level is strongly bound. For example, in HF+D3/3-21++G* simulations such as those described above, for which a stable cavity-bound structure is maintained, the average energy level is $\langle\varepsilon_{SOMO}\rangle = -2.95 \pm 0.42$ eV.[23] Experiments using liquid microjet photoelectron spectroscopy yield vertical ionization energies (VIEs) for e^-(aq) in the range 3.3−3.7

DOI: 10.1021/acs.jpcb.9b04895
J. Phys. Chem. B 2019, 123, 8074−8085

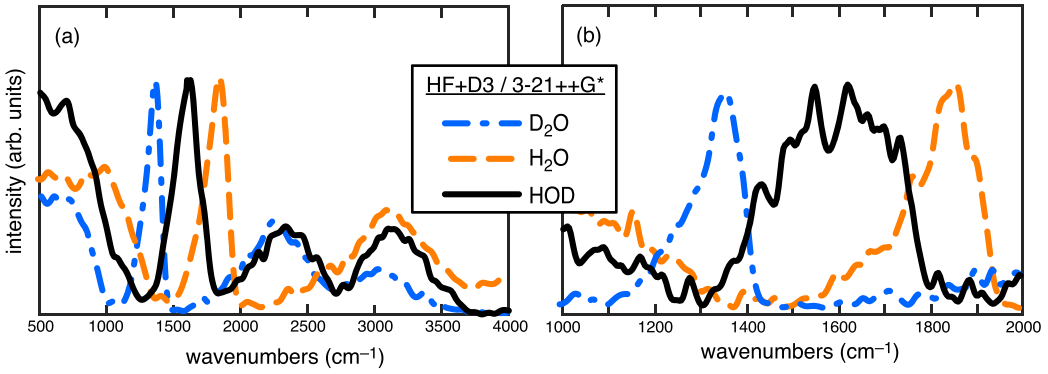

Figure 8. Ensemble-averaged RR intensities for e^-(aq) in isotopically substituted water. (a) Complete spectrum including both bending and stretching regions, with 45 cm^{-1} Lorentzian broadening. (b) Close-up view of the bending region, with 20 cm^{-1} broadening. Calculations were performed at the HF+D3/3-21++G* level based on snapshots from a QM/MM simulation at the same level of theory.

eV,[94−99] with similar values obtained in large water clusters.[100] Similar VIEs are obtained from MP2 calculations performed using UMJ cavity structures, when continuum boundary conditions are used to incorporate long-range polarization effects.[33,101]

Certainly, the VIE need not coincide with ε_{SOMO}. That would be the Koopmans' theorem result, and for ionization energies the errors in this approximation are typically on the order of 0.5−1.0 eV.[85] In view of this, the HF value $\varepsilon_{SOMO} \approx -3.0$ eV that is obtained for cavity structures is perfectly consistent with experiment but a SOMO that is unbound at the HF level, or even marginally bound, is inconsistent with experiment. It simply strains credulity to expect that a molecular orbital with an *unbound* HF energy level actually possesses a VIE > 3 eV.

3.3. Spectra in the Bending Region. In an important set of experiments, Tauber and Mathies[36] measured RR spectra of e^-(aq) in various mixtures of H_2O and D_2O. These experiments reveal a splitting in the bending region of the spectrum when the solvent is HOD, from which the authors conclude that the coordination motif is asymmetric, meaning bond-oriented coordination (O−H···e^-) rather than dipole-oriented (OH_2···e^-) coordination. They furthermore conclude that their results are *inconsistent* with a "solvated solvent anion" model, H_2O^-(aq). The latter has occasionally been offered as a microscopic model of e^-(aq),[93,102,103] but it lacks the asymmetry between hydroxyl groups that is invoked by Tauber and Mathies to explain the splitting of the H−O−D bend.[36] These isotopic substitution experiments have not previously been simulated, nor has the water bending region been considered in previous simulations of the RR spectrum of e^-(aq).

To make contact with the isotopic substitution experiments, we performed QM/MM vibrational frequency calculations at the HF+D3/3-21++G* level, in which all of the H_2O molecules were replaced with D_2O, and also calculations in which all H_2O molecules were replaced with HOD. QM/MM simulations to generate the ensemble were performed in H_2O and then the isotopic substitutions were applied to the snapshots extracted for vibrational frequency calculations. In the HOD calculations, the proton that is deuterated is selected at random so that both HOD···e^- and DOH···e^- coordination should be sampled equally. Note that this rather limited level of theory is certainly not quantitative for vibrational frequencies and that becomes clear when the full, broad-band RR spectrum is compared to experiment; see Figure S4. Nevertheless, the bending feature is unmistakable in our computed spectrum, and what is more important than the absolute vibrational frequencies are the isotopic shifts.

Spectra in D_2O simply exhibit a downshift of ∼1000 cm^{-1} as compared to spectra in H_2O (Figure 8a), but the isotopic mixtures are more interesting. In the experiments of ref 36, a 1:2:1 mixture of D_2O:HOD:H_2O gives rise to three peaks in the bending region, two of which come from isotopically pure water, along with a central peak due to HOD. This is interpreted as a signature of bond-oriented coordination leading to asymmetry between the two hydroxyl groups of water molecules in the first solvation shell.[36]

The 45 cm^{-1} broadening that is used in most of our spectra obscures the splitting in the bending region, although a hint of this splitting can be seen (just above 1500 cm^{-1}) in the HOD spectra that are plotted in Figure 8a. In Figure 8b, the line width is reduced to 20 cm^{-1} in order to reveal a splitting in the H−O−D bend. Spectra computed in H_2O and D_2O both exhibit the same low-energy shoulder, but not the splitting.

The same isotopic substitution protocol was performed on the LGS snapshots, and ensemble-averaged RR spectra (computed at the PBE/3-21++G* level of theory) are reported in Figure S7. These spectra fail to reproduce the splitting in the H−O−D bend, nor do they reproduce the experimental line shape in the O−H (or O−D) stretching region. Instead, the distribution of O−H (or O−D) frequencies is much larger that what is observed either experimentally or in calculations at the cavity-forming HF+D3/3-21++G* level of theory. The spectrum in the stretching region that is computed using LGS geometries is also missing the "two-hump" line shape[36] that is successfully reproduced by the cavity-forming models, as in Figure 8a.

4. SUMMARY AND CONCLUSIONS

Prior to the present work, the RR spectrum of the hydrated electron in the O−H stretching region stood as a prominent example of an experimental result that had been reproduced (at least qualitatively) by non-cavity models of this species, but not within the canonical cavity model.[9,10] The frequency-map approach,[50−53] borrowed from studies of ground-state vibrational spectroscopy of liquid water and used without additional testing in quantum/classical models of e^-(aq),[9,10,12] predicts a downshift of ≈50 cm^{-1} on the low-energy side of the O−H stretching band of the non-cavity hydrated electron. (This shift

DOI: 10.1021/acs.jpcb.9b04895
J. Phys. Chem. B 2019, 123, 8074−8085

is measured with respect to the Raman spectrum of the underlying water model,[9,10] and for comparison the downshift measured experimentally is ≈200 cm^{-1} with respect to the experimental Raman spectrum of neat liquid water.[36]) According to the frequency-map calculations,[9,10] cavity models of e^-(aq) afford RR spectra that are blue-shifted and narrowed relative to the neat solvent, which is opposite to the experimental observations. The detailed reasons for this discrepancy are unclear, although we are suspicious of the frequency-map approach as applied to e^-(aq).

In contrast, the all-electron quantum chemistry calculations that are presented here demonstrate that the main features of the RR spectrum are readily explained within a traditional cavity model. These features include the aforementioned red-shift in the O−H stretching feature, which is somewhat exaggerated in our calculations (≈300 cm^{-1}, versus 200 cm^{-1} in the experiments), but qualitatively reasonable. This shift is present whether we use liquid configurations from cavity or from non-cavity models, suggesting that a sizable red-shift is likely a feature of any semilocalized electron inserted into liquid water. This makes sense given that the red-shift arises from $e^- \rightarrow \sigma^*_{OH}$ charge penetration and is therefore nonspecific as to the details of the spin density. Notably, this is the same mechanism that is responsible for large vibrational red-shifts (up to ≈300 cm^{-1}) that are observed in the infrared spectroscopy of $(H_2O)_n^-$ cluster anions.[1,44]

The bending region of the hydrated electron's RR spectrum has not been considered in previous theoretical studies, perhaps because no frequency map exists for this spectral regime. This region is consider in the present work, and we find that only the cavity geometries are able to reproduce the splitting of the H−O−D bend that is observed experimentally for e^-(aq) in isotopically mixed water.[36] In analyzing their experimental data, Tauber and Mathies[36] cite this splitting as clear evidence that water coordinates to the electron in a bond-oriented fashion (O−H···e^-) that involves a single hydroxyl moiety per solvent molecule. This is consistent with the canonical cavity model but inconsistent with the non-cavity LGS model. The present calculations fully support the interpretation put forward by Tauber and Mathies.

Equally compelling, in our view, is the fact that liquid geometries obtained from the non-cavity LGS model fail to bind an additional electron at the HF+D3/6-31+G* level of theory. In other words, all-electron quantum chemistry predicts that the SOMO energy level of the LGS model is unbound, $\varepsilon_{SOMO} > 0$. To obtain a RR spectrum of e^-(aq) at these non-cavity liquid geometries, we resorted to using the semilocal PBE functional, whose inherent self-interaction error artificially stabilizes ε_{SOMO}. This affords a bound state that can sensibly be used in the RR calculations. However, this observation suggests that, in reality, liquid geometries predicted by the LGS model support only continuum states of an extra electron.

This discrepancy with respect to HF theory is all the more notable in view of the fact that the LGS model was parametrized using the "static-exchange" approximation[40,104,105] to a HF calculation. As noted originally by Turi and Madarász,[3] and recently recapitulated by our group,[23] the numerical fitting of the analytic LGS electron−water interaction potential is not faithful to the underlying quantum chemistry data upon which it is based, and as a result this model overstabilizes the ground-state energy level.[3,7] The net result is that $\varepsilon_{LGS} < 0 < \varepsilon_{SOMO}$. A non-cavity liquid geometry that affords a bound-state LGS wave function ($\varepsilon_{LGS} < 0$), when inserted into a HF calculation, affords an unbound state instead ($\varepsilon_{SOMO} > 0$).

This prediction by the LGS model is inconsistent with experimental photoelectron spectroscopy. Experiments suggest that the VIE of e^-(aq) is 3.3−3.7 eV,[94−100] in good agreement with MP2 calculations carried out on UMJ cavity structures of e^-(aq),[101] upon careful treatment of continuum boundary conditions to incorporate long-range polarization.[33,101] In contrast to the unbound SOMO that is obtained at typical LGS liquid configurations, for the canonical cavity model, one obtains $\varepsilon_{SOMO} \approx -3.0$ eV at the HF level.[23] Such a value is easy to reconcile with the experimental data in view of Koopmans' theorem, and this value is converted to a quantitative VIE when electron correlation and long-range polarization are included.[101]

Overall, quantum chemistry calculations presented here suggest that the conventional cavity model of e^-(aq) is much more consistent with the measured RR spectrum of this species as compared to the non-cavity alternative advocated by Schwartz and co-workers. The conventional model affords a better quantitative description of the O−H red-shift, and only the cavity model reproduces and explains the splitting in the H−O−D bend that is observed in isotopically mixed water. One-electron energy levels obtained for the non-cavity LGS model are wildly inconsistent with the photoelectron spectroscopy of e^-(aq), whereas the cavity model is in good agreement with these data. With regard to the energy levels obtained from the all-electron calculations, we find it impossible to reconcile a SOMO energy level that is *unbound* (by at least 0.5 eV, $\varepsilon_{SOMO} \gtrsim 0.5$ eV) with a VIE ≥ 3.3 eV. To entertain the non-cavity model any further at this point is tantamount to a rejection of either the experimental consensus regarding the VIE,[94−100] or else the notion that quantum chemistry is capable of providing even qualitatively correct one-electron energy levels. A simpler explanation is that a fitting error causes the LGS electron−water pseudopotential to be overly attractive,[3] severely distorting the liquid structures predicted by this model.

■ ASSOCIATED CONTENT

Supporting Information

The Supporting Information is available free of charge on the ACS Publications website at DOI: 10.1021/acs.jpcb.9b04895.

Comparison of broadened and stick spectra, isotropic substitution spectra for the LGS model, and various additional data regarding spin densities obtained from the *ab initio* calculations (PDF)

■ AUTHOR INFORMATION

Corresponding Author

*E-mail: herbert@chemistry.ohio-state.edu.

ORCID

Saswata Dasgupta: 0000-0002-8014-8376

Bhaskar Rana: 0000-0002-8751-7314

John M. Herbert: 0000-0002-1663-2278

Notes

The authors declare the following competing financial interest(s): J.M.H. serves on the Board of Directors of Q-Chem Inc.

DOI: 10.1021/acs.jpcb.9b04895
J. Phys. Chem. B 2019, 123, 8074−8085

■ ACKNOWLEDGMENTS

This work was supported by National Science Foundation Grant No. CHE-1665322, and calculations were performed at the Ohio Supercomputer Center.[106]

■ REFERENCES

(1) Herbert, J. M.; Coons, M. P. The Hydrated Electron. *Annu. Rev. Phys. Chem.* **2017**, *68*, 447−472.
(2) Larsen, R. E.; Glover, W. J.; Schwartz, B. J. Does the Hydrated Electron Occupy a Cavity? *Science* **2010**, *329*, 65−69.
(3) Turi, L.; Madarász, A. Comment on "Does the Hydrated Electron Occupy A Cavity? *Science* **2011**, *331*, 1387.
(4) Jacobson, L. D.; Herbert, J. M. Comment on "Does the Hydrated Electron Occupy a Cavity? *Science* **2011**, *331*, 1387.
(5) Larsen, R. E.; Glover, W. J.; Schwartz, B. J. Response to Comment on "Does the Hydrated Electron Occupy a Cavity? *Science* **2011**, *331*, 1387.
(6) Herbert, J. M.; Jacobson, L. D. Structure of the Aqueous Electron: Assessment of One-Electron Pseudopotential Models in Comparison to Experimental Data and Time-Dependent Density Functional Theory. *J. Phys. Chem. A* **2011**, *115*, 14470−14483.
(7) Turi, L. Hydrated Electrons in Water Clusters: Inside or Outside, Cavity or Noncavity? *J. Chem. Theory Comput.* **2015**, *11*, 1745−1755.
(8) Turi, L. On the Applicability of One- and Many-Electron Quantum Chemistry Models for Hydrated Electron Clusters. *J. Chem. Phys.* **2016**, *144*, 154311.
(9) Casey, J. R.; Larsen, R. E.; Schwartz, B. J. Resonance Raman and Temperature-Dependent Electronic Absorption Spectra of Cavity and Noncavity Models of the Hydrated Electron. *Proc. Natl. Acad. Sci. U. S. A.* **2013**, *110*, 2712−2717.
(10) Casey, J. R.; Kahros, A.; Schwartz, B. J. To Be or Not to Be in a Cavity: The Hydrated Electron Dilemma. *J. Phys. Chem. B* **2013**, *117*, 14173−14182.
(11) Zho, C.-C.; Schwartz, B. J. Time-Resolved Photoelectron Spectroscopy of the Hydrated Electron: Comparing Cavity and Noncavity Models to Experiment. *J. Phys. Chem. B* **2016**, *120*, 12604−12614.
(12) Zho, C.-C.; Farr, E. P.; Glover, W. J.; Schwartz, B. J. Temperature Dependence of the Hydrated Electron's Excited-State Relaxation. I. Simulation Predictions of Resonance Raman and Pump-Probe Transient Absorption Spectra of Cavity and Non-Cavity Models. *J. Chem. Phys.* **2017**, *147*, 074503.
(13) Farr, E. P.; Zho, C.-C.; Challa, J. R.; Schwartz, B. J. Temperature Dependence of the Hydrated Electron's Excited-State Relaxation. II. Elucidating the Relaxation Mechanism through Ultrafast Absorption and Stimulated Emission Spectroscopy. *J. Chem. Phys.* **2017**, *147*, 074504.
(14) Casey, J. R.; Schwartz, B. J.; Glover, W. J. Free Energies of Cavity and Noncavity Hydrated Electrons Near the Instantaneous Air/Water Interface. *J. Phys. Chem. Lett.* **2016**, *7*, 3192−3198.
(15) Glover, W. J.; Schwartz, B. J. Short-Range Electron Correlation Stabilizes Noncavity Solvation of the Hydrated Electron. *J. Chem. Theory Comput.* **2016**, *12*, 5117−5131.
(16) Boero, M.; Parrinello, M.; Terakura, K.; Ikeshoji, T.; Liew, C. C. First-Principles Molecular-Dynamics Simulations of a Hydrated Electron in Normal and Supercritical Water. *Phys. Rev. Lett.* **2003**, *90*, 226403.
(17) Boero, M. Excess Electron in Water at Different Thermodynamic Conditions. *J. Phys. Chem. A* **2007**, *111*, 12248−12256.
(18) Uhlig, F.; Marsalek, O.; Jungwirth, P. Unraveling the Complex Nature of the Hydrated Electron. *J. Phys. Chem. Lett.* **2012**, *3*, 3071−3075. Uhlig, F.; Marsalek, O. Correction to "Unraveling the Complex Nature of the Hydrated Electron". *J. Phys. Chem. Lett.* **2013**, *4*, 603.
(19) Marsalek, O.; Uhlig, F.; Vandevondele, J.; Jungwirth, P. Structure, Dynamics, and Reactivity of Hydrated Electrons by *ab Initio* Molecular Dynamics. *Acc. Chem. Res.* **2012**, *45*, 23−32.
(20) Ambrosio, F.; Miceli, G.; Pasquarello, A. Electronic Levels of Excess Electrons in Liquid Water. *J. Phys. Chem. Lett.* **2017**, *8*, 2055−2059.
(21) Pizzochero, M.; Ambrosio, F.; Pasquarello, A. Picture of the Wet Electron: A Localized Transient State in Liquid Water. *Chem. Sci.* **2019**, *10*, 7442−7448.
(22) Wilhelm, J.; Vandevondele, J.; Rybkin, V. V. Dynamics of the Bulk Hydrated Electron from Many-Body Wave-Function Theory. *Angew. Chem., Int. Ed.* **2019**, *58*, 3890−3893.
(23) Holden, Z. C.; Rana, B.; Herbert, J. M. Analytic Energy Gradients for the QM/MM-Ewald Method Using Atomic Charges Derived from the Electrostatic Potential: Theory, Implementation, and Application to *ab Initio* Molecular Dynamics of the Aqueous Electron. *J. Chem. Phys.* **2019**, *150*, 144115.
(24) Schnitker, J.; Rossky, P. J. Quantum Simulation Study of the Hydrated Electron. *J. Chem. Phys.* **1987**, *86*, 3471−3485.
(25) Rossky, P. J.; Schnitker, J. The Hydrated Electron: Quantum Simulation of Structure, Spectroscopy, and Dynamics. *J. Phys. Chem.* **1988**, *92*, 4277−4285.
(26) Turi, L.; Borgis, D. Analytical Investigations of an Electron−Water Molecule Pseudopotential. II. Development of a New Pair Potential and Molecular Dynamics Simulations. *J. Chem. Phys.* **2002**, *117*, 6186−6195.
(27) Madarász, Á.; Rossky, P. J.; Turi, L. Excess Electron Relaxation Dynamics at Water/Air Interfaces. *J. Chem. Phys.* **2007**, *126*, 234707.
(28) Tay, K. A.; Coudert, F.-X.; Boutin, A. Mechanism and Kinetics of Hydrated Electron Diffusion. *J. Chem. Phys.* **2008**, *129*, 054505.
(29) Tay, K. A.; Boutin, A. Hydrated Electron Diffusion: The Importance of Hydrogen-Bond Dynamics. *J. Phys. Chem. B* **2009**, *113*, 11943−11949.
(30) Jacobson, L. D.; Herbert, J. M. Polarization-Bound Quasi-Continuum States Are Responsible for the 'Blue Tail' in the Optical Absorption Spectrum of the Aqueous Electron. *J. Am. Chem. Soc.* **2010**, *132*, 10000−10002.
(31) Jacobson, L. D.; Herbert, J. M. A One-Electron Model for the Aqueous Electron That Includes Many-Body Electron-Water Polarization: Bulk Equilibrium Structure, Vertical Electron Binding Energy, and Optical Absorption Spectrum. *J. Chem. Phys.* **2010**, *133*, 154506.
(32) Turi, L.; Rossky, P. J. Theoretical Studies of Spectroscopy and Dynamics of Hydrated Electrons. *Chem. Rev.* **2012**, *112*, 5641−5674.
(33) Coons, M. P.; You, Z.-Q.; Herbert, J. M. The Hydrated Electron at The Surface of Neat Liquid Water Appears to Be Indistinguishable from the Bulk Species. *J. Am. Chem. Soc.* **2016**, *138*, 10879−10886.
(34) Tauber, M. J.; Mathies, R. A. Fluorescence and Resonance Raman Spectra of the Aqueous Solvated Electron. *J. Phys. Chem. A* **2001**, *105*, 10952−10960.
(35) Tauber, M. J.; Mathies, R. A. Resonance Raman Spectra and Vibronic Analysis of the Aqueous Solvated Electron. *Chem. Phys. Lett.* **2002**, *354*, 518−526.
(36) Tauber, M. J.; Mathies, R. A. Structure of the Aqueous Solvated Electron from Resonance Raman Spectroscopy: Lessons from Isotopic Mixtures. *J. Am. Chem. Soc.* **2003**, *125*, 1394−1402.
(37) Mizuno, M.; Tahara, T. Novel Resonance Raman Enhancement of Local Structure Around Solvated Electrons in Water. *J. Phys. Chem. A* **2001**, *105*, 8823−8826.
(38) Mizuno, M.; Tahara, T. Picosecond Time-Resolved Resonance Raman Study of the Solvated Electron in Water. *J. Phys. Chem. A* **2003**, *107*, 2411−2421.
(39) Schnitker, J.; Rossky, P. J. An Electron−Water Pseudopotential For Condensed Phase Simulations. *J. Chem. Phys.* **1987**, *86*, 3462−3470.
(40) Turi, L.; Gaigeot, M.-P.; Levy, N.; Borgis, D. Analytical Investigations of an Electron−Water Molecule Pseudopotential. I. Exact Calculations on a Model System. *J. Chem. Phys.* **2001**, *114*, 7805−7815.
(41) Toukan, K.; Rahman, A. Molecular-Dynamics Study of Atomic Motions in Water. *Phys. Rev. B: Condens. Matter Mater. Phys.* **1985**, *31*, 2643−2648.

DOI: 10.1021/acs.jpcb.9b04895
J. Phys. Chem. B 2019, 123, 8074−8085

(42) Thompson, W. H.; Hynes, J. T. Frequency Shifts in the Hydrogen-Bonded OH Stretch in Halide−Water Clusters. The Importance of Charge Transfer. *J. Am. Chem. Soc.* **2000**, *122*, 6278−6286.
(43) Robertson, W. H.; Johnson, M. A. Molecular Aspects of Halide Ion Hydration: The Cluster Approach. *Annu. Rev. Phys. Chem.* **2003**, *54*, 173−213.
(44) Herbert, J. M.; Head-Gordon, M. Charge Penetration and the Origin of Large O−H Vibrational Red-Shifts in Hydrated-Electron Clusters, $(H_2O)_n^-$. *J. Am. Chem. Soc.* **2006**, *128*, 13932−13939.
(45) Neumann, S.; Eisfeld, W.; Sobolewski, A.; Domcke, W. Simulation of the Resonance Raman Spectrum of the Hydrated Electron in the Hydrated-Hydronium Cluster Model. *Phys. Chem. Chem. Phys.* **2004**, *6*, 5297−5303.
(46) Neumann, S.; Eisfeld, W.; Sobolewski, A.; Domcke, W. Simulation of Resonance Raman Spectra of the Solvated Electron in Water and Methanol. In *Femtochemistry VII: Fundamental Ultrafast Processes in Chemistry, Physics, and Biology*; Castleman, A. W., Kimble, M. L., Eds.; Elsevier: Amsterdam, 2006; pp 154−162.
(47) Sobolewski, A. L.; Domcke, W. Hydrated Hydronium: A Cluster Model of the Solvated Electron? *Phys. Chem. Chem. Phys.* **2002**, *4*, 4−10.
(48) Sobolewski, A. L.; Domcke, W. *Ab Initio* Investigation of the Structure and Spectroscopy of Hydronium−Water Clusters. *J. Phys. Chem. A* **2002**, *106*, 4158−4167.
(49) Sobolewski, A. L.; Domcke, W. Computational Studies of Aqueous-Phase Photochemistry and the Hydrated Electron in Finite-Size Clusters. *Phys. Chem. Chem. Phys.* **2007**, *9*, 3818−3829.
(50) Corcelli, S. A.; Lawrence, C. P.; Skinner, J. L. Combined Electronic Structure/Molecular Dynamics Approach for Ultrafast Infrared Spectroscopy of Dilute HOD in Liquid H_2O and D_2O. *J. Chem. Phys.* **2004**, *120*, 8107−8117.
(51) Corcelli, S. A.; Skinner, J. L. Infrared and Raman Line Shapes of Dilute HOD in Liquid H_2O and D_2O from 10 to 90°C. *J. Phys. Chem. A* **2005**, *109*, 6154−6165.
(52) Auer, B.; Kumar, R.; Schmidt, J. R.; Skinner, J. L. Hydrogen Bonding and Raman, IR, and 2D-IR Spectroscopy of Dilute HOD in Liquid D_2O. *Proc. Natl. Acad. Sci. U. S. A.* **2007**, *104*, 14215−14220.
(53) Li, F.; Skinner, J. L. Infrared and Raman Line Shapes for Ice Ih. I. Dilute HOD in H_2O and D_2O. *J. Chem. Phys.* **2010**, *132*, 204505.
(54) Myers, A. B. Resonance Raman Intensities and Charge-Transfer Reorganization Energies. *Chem. Rev.* **1996**, *96*, 911−926.
(55) Silverstein, D. W.; Govind, N.; Van Dam, H. J. J.; Jensen, L. Simulating One-Photon Absorption and Resonance Raman Scattering Spectra Using Analytical Excited State Energy Gradients Within Time-Dependent Density Functional Theory. *J. Chem. Theory Comput.* **2013**, *9*, 5490−5503.
(56) Guthmuller, J. Comparison of Simplified Sum-Over-State Expressions to Calculation Resonance Raman Intensities Including Franck-Condon and Herzberg-Teller Effects. *J. Chem. Phys.* **2016**, *144*, 064106.
(57) Guthmuller, J. Calculation of Vibrational Resonance Raman Spectra of Molecules Using Quantum Chemistry Methods. In *Molecular Spectroscopy: A Quantum Chemistry Approach*; Ozaki, Y., Wójcik, M. J., Popp, J., Eds.; Wiley-Vch: 2019; Vol. *1*, Chapter 17, pp 497−536.
(58) Heller, E. J. The Semiclassical Way to Molecular Spectroscopy. *Acc. Chem. Res.* **1981**, *14*, 368−375.
(59) Heller, E. J.; Sundberg, R. L.; Tannor, D. Simple Aspects of Raman Scattering. *J. Phys. Chem.* **1982**, *86*, 1822−1833.
(60) Myers, A. B.; Mathies, R. A. Resonance Raman Intensities: A Probe of Excited-State Structure and Dynamics. In *Biological Applications of Raman Spectroscopy*; Spiro, T. G., Ed.; Wiley: New York, 1987; Vol. *2*, pp 1−58.
(61) Myers Kelley, A. Resonance Raman and Resonance Hyper-Raman Intensities: Structure and Dynamics of Molecular Excited States in Solution. *J. Phys. Chem. A* **2008**, *112*, 11975−11991.
(62) Petrenko, T.; Neese, F. Analysis and Prediction of Absorption Bandshapes, Fluorescence Bandshapes, Resonance Raman Intensities and Excitation Profiles Using the Time Dependent Theory of Electronic Spectroscopy. *J. Chem. Phys.* **2007**, *127*, 164319.
(63) Petrenko, T.; Neese, F. Efficient and Automatic Calculation of Optical Band Shapes and Resonance Raman Spectra for Larger Molecules within the Independent Mode Displaced Harmonic Oscillator Model. *J. Chem. Phys.* **2012**, *137*, 234107.
(64) Kane, K. A.; Jensen, L. Calculation of Absolute Resonance Raman Intensities: Vibronic Theory vs. Short-Time Approximation. *J. Phys. Chem. C* **2010**, *114*, 5540−5546.
(65) Biczysko, M.; Bloino, J.; Santoro, F.; Barone, V. Time Independent Approaches to Simulate Electronic Spectra Lineshapes: From Small Molecules to Macrosystems. In *Computational Strategies for Spectroscopy, from Small Molecules to Nano Systems*; Barone, V., Ed.; Wiley: Chichester, 2011; Chapter 8, pp 361−443.
(66) Albrecht, A. C. On the Theory of Raman Intensities. *J. Chem. Phys.* **1961**, *34*, 1476−1484.
(67) Tang, J.; Albrecht, A. C. Developments in the Theories of Vibrational Raman Intensities. In *Raman Spectroscopy: Theory and Practice*; Szymanski, H. A., Ed.; Plenum Press: New York, 1970; Vol. *2*, Chapter 2, pp 33−68.
(68) Mingardi, M.; Siebrand, W. Theory of Resonance Raman Scattering. An Improved Formulation of the Vibronic Expansion Method. *J. Chem. Phys.* **1975**, *62*, 1074−1085.
(69) Warshel, A.; Dauber, P. Calculations of Resonance Raman Spectra of Conjugated Molecules. *J. Chem. Phys.* **1977**, *66*, 5477−5488.
(70) Sharp, T. E.; Rosenstock, H. M. Franck−Condon Factors for Polyatomic Molecules. *J. Chem. Phys.* **1964**, *41*, 3453−3463.
(71) Bloino, J.; Baiardi, A.; Biczysko, M. Aiming at an Accurate Prediction of Vibrational and Electronic Spectra for Medium-to-Large Molecules: An Overview. *Int. J. Quantum Chem.* **2016**, *116*, 1543−1574.
(72) Jarzęcki, A. A.; Spiro, T. G. Porphyrin Distortion from Resonance Raman Intensities of Out-of-Plane Modes: Computation and Modeling of *N*-Methylmesoporphyrin, a Ferrochelatase Transition State Analog. *J. Phys. Chem. A* **2005**, *109*, 421−430.
(73) Jarzęcki, A. A. Quantum-Mechanical Calculations of Resonance Raman Intensities: The Weighted-Gradient Approximation. *J. Phys. Chem. A* **2009**, *113*, 2926−2934.
(74) Shao, Y.; et al. Advances in Molecular Quantum Chemistry Contained in the Q-Chem 4 Program Package. *Mol. Phys.* **2015**, *113*, 184−215.
(75) Buchner, M.; Ladanyi, B. M.; Stratt, R. M. The Short-Time Dynamics of Molecular Liquids. Instantaneous-Normal-Mode Theory. *J. Chem. Phys.* **1992**, *97*, 8522−8535.
(76) Stratt, R. M. The Instantaneous Normal Modes of Liquids. *Acc. Chem. Res.* **1995**, *28*, 201−207.
(77) Cho, M.; Fleming, G. R.; Saito, S.; Ohmine, I.; Stratt, R. M. Instantaneous Normal Mode Analysis of Liquid Water. *J. Chem. Phys.* **1994**, *100*, 6672−6683.
(78) Ahlborn, H.; Ji, X.; Space, B.; Moore, P. B. A Combined Instantaneous Normal Mode and Time Correlation Function Description of the Infrared Vibrational Spectrum of Ambient Water. *J. Chem. Phys.* **1999**, *111*, 10622−10632.
(79) Ahlborn, H.; Space, B.; Moore, P. B. The Effect of Isotopic Substitution and Detailed Balance on the Infrared Spectroscopy of Water: A Combined Time Correlation Function and Instantaneous Normal Mode Analysis. *J. Chem. Phys.* **2000**, *112*, 8083−8088.
(80) Yang, C.-Y.; Wong, K. F.; Skaf, M. S.; Rossky, P. J. Instantaneous Normal Mode Analysis of Hydrated Electron Solvation Dynamics. *J. Chem. Phys.* **2001**, *114*, 3598−3611.
(81) Bistafa, C.; Kitamura, Y.; Martins-Costa, M. T. C.; Nagaoka, M.; Ruiz-López, M. F. Vibrational Spectroscopy in Solution Through Perturbative *ab Initio* Molecular Dynamics Simulations. *J. Chem. Theory Comput.* **2019**, *15*, 4615−4622.
(82) Vandevondele, J.; Sprik, M. A Molecular Dynamics Study of the Hydroxyl Radical in Solution Applying Self-Interaction-Corrected Density Functional Methods. *Phys. Chem. Chem. Phys.* **2005**, *7*, 1363−1367.

DOI: 10.1021/acs.jpcb.9b04895
J. Phys. Chem. B 2019, 123, 8074−8085

(83) Grimme, S.; Antony, J.; Ehrlich, S.; Krieg, H. A Consistent And Accurate *ab Initio* Parameterization of Density Functional Dispersion Correction (DFT-D) for the 94 Elements H−Pu. *J. Chem. Phys.* **2010**, *132*, 154104.
(84) Herbert, J. M.; Head-Gordon, M. Calculation of Electron Detachment Energies for Water Cluster Anions: An Appraisal of Electronic Structure Methods, with Application to $(H_2O)_{20}^-$ And. $(H_2O)_{24}^-$. *J. Phys. Chem. A* **2005**, *109*, 5217−5229.
(85) Herbert, J. M. The Quantum Chemistry of Loosely Bound Electrons. In *Reviews in Computational Chemistry*; Parill, A. L., Lipkowitz, K., Eds.; Wiley-VCH: 2015; Vol. *28*, Chapter 8, pp 391−517.
(86) Cohen, A. J.; Mori-Sanchez, P.; Yang, W. Challenges for Density Functional Theory. *Chem. Rev.* **2012**, *112*, 289−320.
(87) Smith, J. D.; Saykally, R. J.; Geissler, P. L. The Effects of Dissolved Halide Anions on Hydrogen Bonding in Liquid Water. *J. Am. Chem. Soc.* **2007**, *129*, 13847−13856.
(88) Ayotte, P.; Bailey, C. G.; Kim, J.; Johnson, M. A. Vibrational Predissociation Spectroscopy of the $(H_2O)_6^-\cdot Ar_n$, $n \geq 6$, Clusters. *J. Chem. Phys.* **1998**, *108*, 444−449.
(89) Hammer, N. I.; Shin, J. W.; Headrick, J. M.; Diken, E. G.; Roscioli, J. R.; Weddle, G. H.; Johnson, M. A. How Do Small Water Clusters Bind an Excess Electron? *Science* **2004**, *306*, 675−679.
(90) Hammer, N. I.; Roscioli, J. R.; Johnson, M. A. Identification of Two Distinct Electron Binding Motifs in the Anionic Water Clusters: A Vibrational Spectroscopic Study of the $(H_2O)_6^-$ Isomers. *J. Phys. Chem. A* **2005**, *109*, 7896−7901.
(91) Hammer, N. I.; Roscioli, J. R.; Johnson, M. A.; Myshakin, E. M.; Jordan, K. D. Infrared Spectrum and Structural Assignment of the Water Trimer Anion. *J. Phys. Chem. A* **2005**, *109*, 11526−11530.
(92) Roscioli, J. R.; Hammer, N. I.; Johnson, M. A. Infrared Spectroscopy of Water Cluster Anions $(H_2O)_{n=3-24}^-$ in the HOH Bending Region: Persistence of the Double H-Bond Acceptor (AA) Water Molecule in the Excess Electron Binding Site of the Class I Isomers. *J. Phys. Chem. A* **2006**, *110*, 7517−7520.
(93) Hameka, H. F.; Robinson, G. W.; Marsden, C. J. Structure of the Hydrated Electron. *J. Phys. Chem.* **1987**, *91*, 3150−3157.
(94) Shreve, A. T.; Yen, T. A.; Neumark, D. M. Photoelectron Spectroscopy of Hydrated Electrons. *Chem. Phys. Lett.* **2010**, *493*, 216−219.
(95) Tang, Y.; Shen, H.; Sekiguchi, K.; Kurahashi, N.; Mizuno, T.; Suzuki, Y. I.; Suzuki, T. Direct Measurement of Vertical Binding Energy of a Hydrated Electron. *Phys. Chem. Chem. Phys.* **2010**, *12*, 3653−3655.
(96) Siefermann, K. R.; Liu, Y.; Lugovoy, E.; Link, O.; Faubel, M.; Buck, U.; Winter, B.; Abel, B. Binding Energies, Lifetimes And Implications of Bulk and Interface Solvated Electrons in Water. *Nat. Chem.* **2010**, *2*, 274−279.
(97) Lübcke, A.; Buchner, F.; Heine, N.; Hertel, I. V.; Schultz, T. Time-Resolved Photoelectron Spectroscopy of Solvated Electrons in Aqueous NaI Solution. *Phys. Chem. Chem. Phys.* **2010**, *12*, 14629−14634.
(98) Yamamoto, Y.; Karashima, S.; Adachi, S.; Suzuki, T. Wavelength Dependence of UV Photoemission from Solvated Electrons in Bulk Water, Methanol, and Ethanol. *J. Phys. Chem. A* **2016**, *120*, 1153−1159.
(99) Luckhaus, D.; Yamamoto, Y.; Suzuki, T.; Signorell, R. Genuine Binding Energy of the Hydrated Electron. *Sci. Adv.* **2017**, *3*, e1603224.
(100) Gartmann, T. E.; Ban, L.; Yoder, B. L.; Hartweg, S.; Chasovskikh, E.; Signorell, R. Relaxation Dynamics and Genuine Properties of the Solvated Electron in Neutral Water Clusters. *J. Phys. Chem. Lett.* **2019**, *10*, 4777−4782.
(101) Coons, M. P.; Herbert, J. M. Quantum Chemistry in Arbitrary Dielectric Environments: Theory and Implementation of Non-equilibrium Poisson Boundary Conditions and Application to Compute Vertical Ionization Energies at the Air/Water Interface. *J. Chem. Phys.* **2018**, *148*, 222834.
(102) Symons, M. C. R. Solvated Electrons or Solvated Solvent Anions? *Radiat. Phys. Chem.* **1981**, *17*, 425−429.
(103) Tuttle, T. R., Jr.; Golden, S. Solvated Electrons: What Is Solvated? *J. Phys. Chem.* **1991**, *95*, 5725−5736.
(104) Smallwood, C. J.; Larsen, R. E.; Glover, W. J.; Schwartz, B. J. A Computationally Efficient Exact Pseudopotential Method. I. Analytic Reformulation of the Phillips-Kleinman Theory. *J. Chem. Phys.* **2006**, *125*, 074102.
(105) Jacobson, L. D.; Williams, C. F.; Herbert, J. M. The Static-Exchange Electron-Water Pseudopotential, in Conjunction with a Polarizable Water Model: A New Hamiltonian for Hydrated-Electron Simulations. *J. Chem. Phys.* **2009**, *130*, 124115.
(106) Ohio Supercomputer Center (http://osc.edu/ark:/19495/f5s1ph73).

DOI: 10.1021/acs.jpcb.9b04895
J. Phys. Chem. B 2019, 123, 8074−8085